A&A 496, 441–451 (2009)
DOI: 10.1051/0004-6361/200810995

Astronomy & Astrophysics

Membership and lithium in the old, metal-poor open cluster Berkeley 32⋆

S. Randich[1], G. Pace[1,2], L. Pastori[3], and A. Bragaglia[4]

[1] INAF/Osservatorio Astrofisico di Arcetri, Largo E. Fermi 5, 50125 Firenze, Italy
e-mail: randich@arcetri.astro.it
[2] Centro de Astrofisica, Universidade de Porto, Rua das Estrellas, 4150-762 Porto, Portugal
[3] INAF/Osservatorio Astronomico di Brera, via E. Bianchi 46, 23807, Italy
[4] INAF/Osservatorio Astronomico di Bologna, via Ranzani 1, 40127 Bologna, Italy

Received 19 September 2008 / Accepted 18 November 2008

ABSTRACT

Context. Measurements of lithium (Li) abundances in open clusters provide a unique tool for following the evolution of this element with age, metallicity, and stellar mass. In spite of the plethora of Li data already available, the behavior of Li in solar-type stars has so far been poorly understood.
Aims. Using FLAMES/Giraffe on the VLT, we obtained spectra of 157 candidate members of the old, metal-poor cluster Berkeley 32, to determine membership and to study the Li behavior of confirmed members.
Methods. Radial velocities were measured, allowing us to derive both the cluster velocity and membership information for the sample stars. The Li abundances were obtained from the equivalent width of the Li I 670.8 nm feature, using curves of growth.
Results. We obtained an average radial velocity of 105.2 ± 0.86 km s^{-1}, and 53% of the stars have a radial velocity consistent with membership. The Li – $T_{\rm eff}$ distribution of unevolved members matches the upper envelope of M 67, as well as that of the slightly older and more metal-rich NGC 188. No major dispersion in Li is detected. When considering the Li distribution as a function of mass, however, Be 32 members with solar-like temperature are less massive and less Li-depleted than their counterparts in the other clusters. The mean Li of stars in the temperature interval 5750 ≤ $T_{\rm eff}$ ≤ 6050 K is log n(Li) = 2.47 ± 0.16, less than a factor of two below the average Li of the 600 Myr old Hyades, and slightly above the average of intermediate age (1–2 Gyr) clusters, the upper envelope of M 67, and NGC 188. This value is comparable to or slightly higher than the plateau of Pop. II stars. The similarity of the average Li abundance of clusters of different age and metallicity, along with its closeness to the halo dwarf plateau, is very intriguing and suggests that, whatever the initial Li abundance and the Li depletion histories, old stars converge to almost the same final Li abundance.

Key words. stars: abundances – stars: evolution – stars: interiors – open clusters and associations: individual: Berkeley 32

1. Introduction

Despite its low abundance (N(Li)/N(H) ≤ 2×10^{-9}), lithium (Li) plays a fundamental role in different fields of astrophysics because of how it is created and destroyed. The ^{7}Li isotope is the heaviest element produced during big bang nucleosynthesis (BBN), and its primordial abundance strongly depends on η, the ratio of baryons to photons (e.g., Steigman 2006, and references therein). At the same time, Li is easily depleted from stellar atmospheres: ^{7}Li is destroyed by proton reactions at the relatively low temperature of ∼2.5 MK, implying depletion with respect to the initial content whenever a mixing process is present that is able to transport surface material down to the deeper regions in the stellar interior where this temperature is reached.

Primordial Li abundance has been empirically estimated by means of Li measurements in old Pop. II stars and, theoretically, using BBN calculations combined with the baryon density derived from measurements of the cosmic microwave background temperature fluctuations. The reliability of the latter has dramatically improved after data from the WMAP satellite became available (Cyburt et al. 2003; Spergel et al. 2007). Estimates from old stars rely on the assumption that the hot ($T_{\rm eff}$ ≥ 5800 K), metal poor, Pop. II dwarfs do not deplete Li in their atmosphere, hence represent the primordial material from which they were born. The confidence on this assumption is based on the near constancy of their Li abundance with metallicity, first discovered by Spite & Spite (1982) and generally referred to as the Spite plateau. Primordial Li abundance predicted from standard BBN calculations with WMAP is a factor of two to three higher than that of the Spite plateau, which might indicate that halo stars have indeed undergone some Li depletion, possibly due to microscopic diffusion, as recently claimed by Korn et al. (2006, 2007). Only through a full understanding of mixing inside stars and its dependence on metallicity will we be able to reach a conclusion with complete confidence.

To achieve that, studies in Pop. I stars, and in particular among open cluster members, are the most suitable observation tool. Lithium (and beryllium) measurements in Galactic open clusters (OCs) indeed allow us to empirically trace Li depletion with age, metallicity, and mass. Focusing on solar-type stars, standard models of stellar evolution (those including convection only) predict that these stars should not suffer any Li depletion during the main sequence (MS), since their convective zone does not reach the Li burning layer. Surveys of Li in a variety of OCs and, in particular, the comparison of the Li patterns

⋆ Based on observations collected at ESO-VLT, Paranal Observatory, Chile, Program number 74.D-0571(A).

of OCs of different age, have shown that, at variance with these predictions, solar-type stars do deplete Li on the MS. Depletion starts at ∼100 Myr and smoothly goes on up to the Hyades age, on a timescale of ∼1.4 Gyr. After that age depletion becomes bimodal: it is very fast for a fraction of stars, like the Sun itself, and the lower envelope of M 67 (Pasquini et al. 1997, and references therein), while depletion completely stops after ∼1 Gyr for a significant fraction of stars (Sestito & Randich 2005; Prisinzano & Randich 2007) In particular, Randich et al. (2003 -RSP03 hereafter) have shown that members of the old (6–8 Gyr) OC NGC 188 have a Li abundance only a factor of two smaller than their counterparts in the factor of 10 younger Hyades; moreover, the average value of Li in NGC 188 is surprisingly close to what is measured in Pop. II stars. This open cluster has a solar metallicity and, as discussed by RSP03, this result might be a mere coincidence; however, the issue is obviously worth further studies. It might indeed represent a link between Pop. I and Pop. II. Li depletion histories and provide a clue to understand whether the latter have undergone Li depletion. Investigating Li in additional very old OCs is thus very important.

It is worth mentioning that, to explain the unexpected Li depletion during the MS, several non-standard processes were included in the models. The proposed mechanisms include diffusion (Michaud 1986; Michaud et al. 2004; Chaboyer et al. 1995), meridional circulation (Charbonnel & Talon 1999, and references therein), angular momentum loss and rotationally driven mixing (Eddington 1925; Zahn 1974, 1992; Deliyannis & Pinsonneault 1997), gravity waves (García López & Spruit 1991; Montalbàn & Schatzmann 2000), tachocline (Spergel & Zahn 1992; Brun et al. 1999; Piau et al. 2003), and combinations of waves and rotation (Charbonnel & Talon 2005; Talon 2008). Each of these models makes specific predictions on the timescales of Li depletion which can be compared with observational patterns.

We present here Li observations in a very large sample of members of Berkeley 32. This open cluster is one of the oldest in the Galaxy (5 Gyr – e.g. D' Orazi et al. 2006) and its metallicity is a factor of two below solar (Sestito et al. 2006); therefore, it provides an ideal sample to further investigate the issue of the convergence of Li at old ages.

The paper is organized as follows. In Sect. 2 we describe the sample, the observations, and data reduction. Data analysis and the results are presented in Sects. 3 and 4. A discussion is provided in Sect. 5, followed by conclusions in Sect. 6.

2. Sample and observations

The observations were obtained with VLT/FLAMES. Specifically, we used the fiber link to UVES to acquire spectra of evolved stars (RGB and clump stars) to be used for the determination of the cluster chemical compositions (Sestito et al. 2006; Bragaglia et al. 2008), while the Giraffe spectrograph and Medusa fiber system were employed to observe MS and/or turn-off (TO) cluster candidates as well as a few subgiants, in order to derive membership and information on Li.

2.1. Targets

Photometric surveys of Be 32 have been performed by Kaluzny & Mazur (1991), Richtler & Sagar (2000), Hasegawa et al. (2004), and D' Orazi et al. (2006). A re-analysis of D' Orazi et al. photometry was performed by Tosi et al.(2007). All these studies agree on a cluster age of 5–6 Gyr, on a subsolar metallicity,

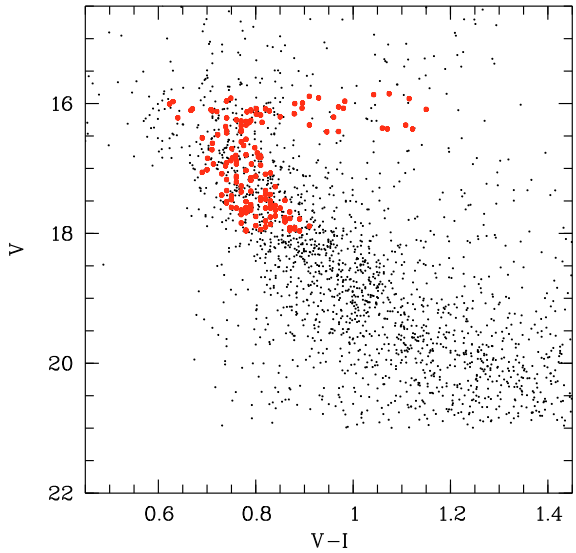

Fig. 1. V vs. $V - I$ diagram of Be 32 with FLAMES targets shown as filled symbols. The whole catalog was constructed using Richtler & Sagar (2000) photometry. We show in the figure only stars brighter than $V = 21$.

and on a reddening E($B - V$) in the range 0.08–0.16, with a most likely value of 0.1–0.12 (see discussion in Tosi et al.). Based on UVES spectra of nine cluster members Sestito et a. (2006) derived for the cluster a metallicity [Fe/H] = −0.29 ± 0.04. So far no spectroscopic studies of MS stars have been performed and membership is based only on photometric criteria.

We selected Giraffe target stars from the catalogs of Kaluzny & Mazur (1991) and Richtler & Sagar (2000), since the study of D'Orazi et al. was still in preparation at the time of the observations. The $V - V - I$ diagram of the target stars is displayed in Fig. 1 which shows that the sample includes stars from the cluster subgiant branch and turn-off (TO) ($V \sim 16$) down to $V = 18$. As mentioned, membership for these candidates so far has been based only on photometry. One of the purposes of this study is a more reliable determination of membership via radial velocity measurements.

2.2. Observations and data reduction

Be 32 was observed with two different FLAMES configurations (A and B) centered at RA(2000) = $06^h58^m04.2^s$ and Dec(2000) = $-06^d28^m21.1^s$ and RA(2000) = $06^h58^m02.0^s$ and Dec(2000) = $-06^d22^m41.4^s$, respectively. We obtained four and one 3600 s long exposures for configurations A and B, respectively. Observations were obtained in Visitor mode on Jan. 20, 2005 (configuration A) and Jan. 21, 2005 (configuration B). Medusa fibers were allocated to 112 and 108 objects in the two configurations, with 63 stars in common. In total we thus obtained spectra of 157 cluster candidates. In both configurations 15 fibers were put on the sky. Stars covered by configurations A and B were observed for a total of 4 and 1 h, respectively, while the 63 stars in common were observed for 5 h. Target stars, together with their photometry, are listed in Table 1. In the table we list our running ID (Col. 1), coordinates from Kaluzny & Mazur (1991) if the star is present in their catalog otherwise from Richtler & Sagar (2000 – Cols. 2, 3); photometry from D' Orazi et al. (2006 – Cols. 4–7); V magnitude from Kaluzny & Mazur (1991) if the star is present in their catalog otherwise from Richtler & Sagar (2000 – Col. 8); $B - V$ from Kaluzny & Mazur (Col. 9); $V - I$ from Richtler & Sagar (Col. 10); radial

Table 1. Sample stars.

ID	RA J2000	Dec	Conf.	$B_{\rm DBT}$	$V(B-V)_{\rm DBT}$	$V(V-I)_{\rm DBT}$	$I_{\rm DBT}$	$V_{\rm lit.}$	$B-V_{\rm KM}$	$V-I_{\rm RS}$	$v_{\rm rad}$ (km s^{-1})	mf
74	6 58 05.410	6 25 40.18	B	16.840	15.846	15.855	14.798	15.862	0.956	1.042	105.4 ± 1.5	m
77	6 57 56.856	6 24 26.47	B	–	–	–	–	15.889	0.871	0.910	–	?
84	6 58 09.005	6 28 55.83	A	16.567	15.953	15.948	15.196	15.955	0.598	0.742	44.7 ± 2.4	n
86	6 58 05.060	6 24 59.35	A	16.536	15.987	15.983	15.317	15.972	0.544	0.628	111.5 ± 0.94	n
91	6 58 00.353	6 27 44.37	A	16.745	15.969	15.970	15.082	16.001	0.744	0.883	33.6 ± 0.14	n
97	6 58 14.083	6 26 43.18	A	16.930	16.060	16.060	15.056	16.052	0.872	0.975	104.8 ± 0.43	m
99	6 58 00.174	6 26 39.60	B	16.862	16.073	16.073	15.161	16.069	0.781	0.895	107.1 ± 1.2	m
101	6 58 06.636	6 24 12.65	B	16.938	16.048	16.051	15.059	16.074	0.867	0.980	34.1 ± 0.9	n
106	6 58 04.028	6 24 08.09	A	16.807	16.108	16.108	15.303	16.099	0.717	0.786	50.1 ± 0.43	n
109	6 58 18.702	6 27 03.72	A	16.711	16.049	16.041	15.203	16.106	0.668	0.794	104.2 ± 0.32	m
110	6 57 54.792	6 28 22.07	B	16.698	16.042	16.032	15.183	16.112	0.649	0.828	106.4 ± 2.2	m
111	6 57 53.981	6 24 23.93	B	16.749	16.106	16.102	15.315	16.120	0.620	0.805	106.3 ± 2	m
117	6 58 13.277	6 26 02.88	B	16.943	16.133	16.136	15.225	16.156	0.766	0.879	104.7 ± 1.2	m
122	6 58 14.152	6 29 31.54	A	16.992	16.180	16.176	15.199	16.207	0.823	0.955	105.3 ± 0.25	m
127	6 58 08.191	6 24 35.48	A	16.868	16.247	16.243	15.483	16.249	0.603	0.755	96.5 ± 1.25	n
130	6 57 56.913	6 27 16.87	A	16.890	16.260	16.254	15.470	16.267	0.618	0.765	105.0 ± 0.28	m
137	6 58 15.058	6 26 40.60	B	17.335	16.286	16.291	15.136	16.333	1.019	1.108	49.7 ± 1.4	n
146	6 58 03.057	6 24 31.69	A	17.062	16.441	16.437	15.680	16.414	0.629	0.766	105.2 ± 0.32	m
147	6 58 17.988	6 29 43.94	A	16.961	16.401	16.388	15.612	16.426	0.586	0.744	96.2 ± 0.59	n
148	6 58 04.879	6 27 39.04	A	17.033	16.411	16.406	15.646	16.435	0.588	0.770	71.1 ± 0.16	n
154	6 58 16.781	6 26 11.06	B	17.058	16.459	16.452	15.695	16.481	0.583	0.722	104.5 ± 2.4	m
169	6 58 07.185	6 23 48.59	B	17.206	16.626	16.620	15.891	16.613	0.579	0.711	–	?
189	6 57 58.952	6 26 48.52	B	17.458	16.798	16.792	15.970	16.762	0.662	0.803	105.2 ± 1.4	m
193	6 58 02.247	6 29 21.35	A	17.362	16.768	16.759	15.981	16.785	0.605	0.780	104.9 ± 0.84	m
202	6 58 03.561	6 23 46.77	B	17.459	16.845	16.838	16.058	16.835	0.617	0.752	107.1 ± 3.1	m
206	6 58 14.715	6 27 02.31	B	17.431	16.814	16.808	16.044	16.844	0.604	0.701	107.1 ± 2	m
212	6 58 12.503	6 28 33.07	B	17.469	16.873	16.863	16.079	16.879	0.605	0.749	63.3 ± 2.1	n
213	6 58 16.427	6 23 34.95	B	17.450	16.848	16.841	16.072	16.881	0.605	0.760	103.3 ± 1.9	m
216	6 57 54.890	6 27 12.27	A	17.473	16.903	16.888	16.088	16.909	0.570	0.741	104.8 ± 1.3	m
218	6 58 04.891	6 23 31.10	B	17.543	16.944	16.936	16.169	16.929	0.627	0.713	108.6 ± 3.6	n
219	6 58 15.312	6 28 15.59	A	17.520	16.886	16.877	16.067	16.929	0.632	0.760	110.8 ± 0.8	n
220	6 58 10.153	6 23 51.84	B	17.561	16.918	16.913	16.120	16.930	0.633	0.791	81.3 ± 3.0	n
222	6 58 16.404	6 27 15.53	B	17.509	16.903	16.895	16.125	16.960	0.571	0.738	105.3 ± 2.4	m
231	6 58 14.010	6 26 57.99	A,B	17.589	16.983	16.977	16.222	17.019	0.589	0.695	104.8 ± 1.0	m
236	6 58 02.398	6 26 57.18	A	–	–	–	–	17.065	0.704	0.833	105.5 ± 0.57	m
240	6 58 12.220	6 25 57.42	A,B	17.797	17.073	17.078	16.292	17.124	0.658	0.804	35.6 ± 1.1	n
241	6 57 57.665	6 25 41.09	A,B	17.773	17.152	17.146	16.371	17.135	0.591	0.759	105.8 ± 0.54	m
245	6 58 02.865	6 25 09.94	A,B	–	–	–	–	17.167	0.616	0.737	110.6 ± 0.4	n
254	6 58 01.182	6 29 00.09	A	17.925	17.257	17.249	16.403	17.279	0.674	0.835	45.7 ± 1.0	n
265	6 58 12.307	6 24 50.80	A,B	18.004	17.334	17.336	16.586	17.342	0.679	0.737	104.7 ± 1.2	m
271	6 58 16.474	6 24 00.78	A,B	17.955	17.317	17.312	16.529	17.355	0.641	0.770	105.2 ± 1.11	m
276	6 57 58.540	6 28 06.48	A,B	18.020	17.376	17.368	16.543	17.396	0.649	0.823	104.8 ± 0.32	m
277	6 57 53.234	6 27 03.85	A,B	18.046	17.440	17.427	16.609	17.398	0.513	0.831	104.8 ± 0.7	m
278	6 58 06.158	6 26 01.56	A,B	18.075	17.419	17.418	16.652	17.410	0.643	0.734	104.7 ± 1.92	m
288	6 58 08.217	6 26 28.77	A,B	18.137	17.414	17.417	16.619	17.447	0.636	0.806	107.6 ± 0.6	m
289	6 58 05.985	6 25 23.23	A,B	18.154	17.447	17.445	16.615	17.454	0.670	0.807	105.6 ± 0.9	m
292	6 58 06.568	6 26 53.29	A,B	18.103	17.470	17.465	16.691	17.485	0.579	0.752	92.5 ± 1.0	n
294	6 58 15.206	6 29 36.09	A,B	18.115	17.464	17.458	16.644	17.491	0.677	0.814	63.6 ± 1.0	n
299	6 58 01.374	6 27 16.75	A,B	18.206	17.524	17.521	16.712	17.512	0.645	0.777	105.3 ± 1.3	m
311	6 58 05.745	6 23 45.05	A	18.263	17.577	17.569	16.697	17.573	0.686	0.828	104.1 ± 0.5	m
313	6 58 06.532	6 25 38.80	A,B	18.282	17.571	17.580	16.845	17.597	0.635	0.751	105.1 ± 1.1	m
314	6 58 10.331	6 27 12.53	A,B	18.208	17.575	17.566	16.754	17.602	0.616	0.794	107.6 ± 0.6	m
315	6 58 00.111	6 27 07.30	A	18.287	17.601	17.596	16.757	17.607	0.600	0.822	105.7 ± 1.3	m
316	6 58 10.618	6 24 23.52	A,B	18.276	17.608	17.606	16.810	17.610	0.670	0.761	105.8 ± 0.5	m
317	6 58 16.862	6 26 32.37	A,B	18.301	17.591	17.584	16.691	17.612	0.694	0.850	110.0 ± 1.6	n
325	6 57 55.799	6 28 12.39	A,B	18.257	17.584	17.575	16.717	17.635	0.671	0.840	105.3 ± 0.6	m
326	6 58 17.239	6 23 49.38	A,B	18.222	17.610	17.601	16.812	17.645	0.625	0.771	114.1 ± 1.13	n
331	6 58 06.080	6 26 36.12	A,B	18.392	17.684	17.688	16.911	17.679	0.692	0.784	46.7 ± 2	n
333	6 58 14.218	6 25 31.96	A	–	–	–	–	17.707	0.680	0.765	104.8 ± 0.7	m
344	6 57 58.305	6 25 58.35	A	18.503	17.792	17.790	16.946	17.768	0.707	0.873	100.1 ± 1.0	n
352	6 58 18.582	6 29 32.81	A,B	18.436	17.768	17.760	16.913	17.808	0.678	0.819	104.5 ± 1	m
357	6 58 00.620	6 24 29.96	A,B	18.569	17.878	17.879	17.094	17.839	0.677	0.773	104.5 ± 1.5	m
362	6 58 10.854	6 26 43.75	A,B	–	–	–	–	17.878	0.625	0.797	51.7 ± 5	n

Table 1. continued.

ID	RA	Dec	Conf.	$B_{\rm DBT}$	$V(B-V)_{\rm DBT}$	$V(V-I)_{\rm DBT}$	$I_{\rm DBT}$	$V_{\rm lit.}$	$B-V_{\rm KM}$	$V-I_{\rm RS}$	$v_{\rm rad}$	mf
	J2000										(km s^{-1})	
364	6 58 04.497	6 26 55.95	A,B	18.666	17.897	17.909	17.138	17.880	0.723	0.803	105.4 ± 1.2	m
367	6 58 09.763	6 23 37.42	A,B	18.523	17.889	17.876	17.029	17.896	0.658	0.820	40.5 ± 0.3	n
369	6 57 54.006	6 24 58.68	A,B	18.650	17.955	17.955	17.149	17.910	0.755	0.879	103.4 ± 1.0	m
371	6 57 58.413	6 23 49.71	A,B	18.652	17.941	17.939	17.103	17.934	0.723	0.877	106.0 ± 0.8	m
373	6 57 59.759	6 23 29.26	A,B	18.602	17.937	17.935	17.149	17.952	0.609	0.777	70.2 ± 1.5	n
374	6 58 10.035	6 26 56.43	A	18.670	17.947	17.947	17.118	17.965	0.669	0.775	105.2 ± 0.7	m
927	6 58 05.163	6 23 01.21	A	14.268	12.889	12.904	11.461	12.896	–	1.425	105.5 ± 0.3	m
1043	6 58 11.169	6 22 14.52	B	16.785	15.841	15.845	14.794	15.848	–	1.074	37.2 ± 1.6	n
1047	6 57 51.082	6 20 53.46	B	–	–	–	–	15.912	–	0.929	104.9 ± 2.3	m
1049	6 58 03.201	6 21 12.02	B	–	–	–	–	15.917	–	0.749	43.5 ± 6.3	n
1050	6 58 03.329	6 22 25.01	B	16.887	15.894	15.899	14.805	15.923	–	1.115	105.3 ± 1.2	m
1051	6 58 28.829	6 20 59.65	B	–	–	–	–	15.964	–	0.983	–	?
1057	6 58 20.765	6 22 07.75	B	16.761	16.007	16.006	15.131	15.991	–	0.896	42.0 ± 2.1	n
1059	6 57 44.117	6 24 57.58	B	–	–	–	–	16.006	–	0.623	106.8 ± 3.8	m
1066	6 58 24.787	6 24 09.94	B	16.756	16.082	16.077	15.260	16.077	–	0.801	105.5 ± 1.2	m
1069	6 57 52.859	6 29 07.52	A	–	–	–	–	16.082	–	0.668	99.5 ± 1.6	n
1070	6 58 04.031	6 22 57.96	A	16.728	16.066	16.060	15.243	16.083	–	0.818	104.8 ± 0.3	m
1072	6 58 23.376	6 27 00.93	A	17.113	16.090	16.091	14.924	16.089	–	1.153	51.8 ± 0.2	n
1073	6 57 43.108	6 22 07.05	B	–	–	–	–	16.095	–	0.708	69.7 ± 5.6	n
1074	6 58 19.457	6 22 01.50	B	16.640	16.128	16.123	15.480	16.103	–	0.667	58.9 ± 1.4	n
1075	6 58 21.900	6 22 13.24	A	16.662	16.126	16.119	15.425	16.108	–	0.711	27.0 ± 1.1	n
1077	6 58 26.626	6 30 12.54	B	–	–	–	–	16.123	–	0.720	106.5 ± 1.8	m
1078	6 57 51.039	6 29 04.62	B	–	–	–	–	16.127	–	0.782	14.6 ± 5.2	n
1082	6 58 27.554	6 24 16.90	B	–	–	–	–	16.163	–	0.801	–	?
1084	6 58 10.628	6 20 40.14	B	–	–	–	–	16.177	–	0.810	104.4 ± 1.7	m
1088	6 57 52.147	6 29 18.22	B	–	–	–	–	16.204	–	0.850	105.8 ± 2.0	m
1090	6 58 14.337	6 22 57.76	A	16.726	16.223	16.217	15.573	16.216	–	0.638	106.5 ± 4.5	m, SB2?
1092	6 58 23.454	6 28 52.21	A	16.844	16.231	16.225	15.462	16.220	–	0.744	105.2 ± 0.6	m
1097	6 58 10.641	6 30 41.64	A	16.819	16.250	16.233	15.414	16.258	–	0.789	104.6 ± 0.2	m
1101	6 57 54.904	6 22 58.15	B	16.858	16.238	16.232	15.462	16.275	–	0.780	105.5 ± 1.3	m
1102	6 58 15.248	6 21 37.54	B	16.962	16.363	16.346	15.495	16.289	–	0.813	84.7 ± 2.9	n
1105	6 58 03.716	6 20 16.81	B	–	–	–	–	16.300	–	0.784	103.9 ± 1.7	m
1112	6 58 20.650	6 31 00.58	B	–	–	–	–	16.330	–	0.913	39.9 ± 0.5	n
1113	6 58 20.285	6 23 48.40	A	16.947	16.335	16.329	15.565	16.333	–	0.775	104.9 ± 0.7	m
1114	6 57 51.759	6 27 17.88	A	16.922	16.342	16.329	15.541	16.336	–	0.769	101.7 ± 0.9	n
1116	6 57 45.696	6 24 02.85	B	–	–	–	–	16.354	–	0.738	75.0 ± 5.9	n
1117	6 57 51.055	6 31 13.59	A	–	–	–	–	16.376	–	1.065	105.0 ± 0.2	m
1121	6 58 03.681	6 22 17.30	A	17.255	16.362	16.361	15.319	16.386	–	1.067	104.8 ± 0.4	m
1122	6 58 24.188	6 21 04.34	B	–	–	–	–	16.393	–	1.122	43.4 ± 1.6	n
1123	6 58 21.389	6 30 32.08	A	–	–	–	–	16.420	–	0.741	54.1 ± 0.4	n
1126	6 57 59.971	6 30 05.96	A	17.171	16.353	16.352	15.395	16.431	–	0.966	17.9 ± 0.5	n
1128	6 58 30.891	6 23 30.75	B	–	–	–	–	16.434	–	0.738	105.0 ± 1.0	m
1129	6 57 50.796	6 27 03.39	B	17.300	16.481	16.476	15.482	16.435	–	0.946	58.7 ± 2.7	n
1130	6 58 14.736	6 31 19.87	A	–	–	–	–	16.450	–	0.740	107.3 ± 0.4	m
1141	6 58 20.329	6 30 36.64	A	–	–	–	–	16.531	–	0.693	105.2 ± 0.5	m
1144	6 57 50.902	6 21 57.44	A	–	–	–	–	16.555	–	0.776	59.5 ± 0.3	n
1150	6 58 10.245	6 21 06.25	A	–	–	–	–	16.590	–	0.774	106.1 ± 0.8	m
1153	6 58 09.489	6 21 07.21	B	–	–	–	–	16.629	–	0.787	104.5 ± 2.9	m
1156	6 57 51.474	6 22 38.53	B	–	–	–	–	16.646	–	0.775	106.0 ± 2.2	m
1161	6 57 48.933	6 22 14.65	B	–	–	–	–	16.695	–	0.751	62.2 ± 3.0	n
1164	6 58 25.577	6 29 39.85	A	–	–	–	–	16.707	–	0.711	95.9 ± 0.2	n
1179	6 58 17.498	6 20 46.12	B	–	–	–	–	16.799	–	0.759	35.4 ± 4.4	n
1181	6 57 54.593	6 21 30.34	A	–	–	–	–	16.809	–	0.808	−15.8 ± 1.0	n
1187	6 58 21.059	6 24 31.50	A	17.561	16.853	16.851	16.015	16.829	–	0.814	34.9 ± 0.3	n
1195	6 58 20.695	6 19 17.52	B	–	–	–	–	16.880	–	0.798	104.4 ± 1.7	m
1212	6 58 06.229	6 29 45.40	A	17.587	16.972	16.960	16.140	16.955	–	0.806	104.2 ± 0.9	m
1228	6 57 51.634	6 27 48.18	A,B	17.675	17.070	17.056	16.224	17.028	–	0.776	105.1 ± 0.8	m
1231	6 57 57.805	6 30 26.93	A,B	17.636	17.039	17.027	16.227	17.060	–	0.693	105.8 ± 1.4	m
1238	6 57 53.881	6 22 43.21	A,B	–	–	–	–	17.077	–	0.734	98.2 ± 1.5	n
1241	6 57 52.746	6 26 48.95	A,B	17.607	17.109	17.083	16.260	17.087	–	0.816	105.4 ± 0.6	m
1245	6 58 08.660	6 21 11.52	A,B	–	–	–	–	17.116	–	0.762	40.3 ± 0.9	n
1250	6 57 46.565	6 23 34.51	A,B	–	–	–	–	17.143	–	0.789	64.7 ± 0.8	n
1257	6 58 06.810	6 21 30.85	A,B	–	–	–	–	17.172	–	0.785	105.1 ± 0.3	m
1263	6 58 11.569	6 31 06.92	A,B	–	–	–	–	17.183	–	0.794	104.4 ± 1.5	m

Table 1. continued

ID	RA J2000	Dec	Conf.	B_{DBT}	$V(B-V)_{DBT}$	$V(V-I)_{DBT}$	I_{DBT}	$V_{lit.}$	$B-V_{KM}$	$V-I_{RS}$	v_{rad} (km s^{-1})	mf
1265	6 58 25.849	6 20 00.02	A,B	–	–	–	–	17.214	–	0.763	48.9 ± 1.2	n
1279	6 58 19.836	6 24 48.43	A,B	17.926	17.285	17.282	16.517	17.268	–	0.770	105.6 ± 0.4	m
1300	6 58 24.200	6 26 52.86	A	18.032	17.399	17.385	16.530	17.338	–	0.817	103.0 ± 1.2	m
1302	6 58 23.298	6 24 22.61	A,B	17.976	17.374	17.366	16.588	17.350	–	0.791	79.6 ± 0.3	n
1327	6 58 19.564	6 26 46.99	A,B	18.110	17.454	17.447	16.629	17.419	–	0.749	104.9 ± 0.2	m
1337	6 58 20.259	6 22 51.31	A	18.130	17.500	17.490	16.666	17.474	–	0.824	105.1 ± 1.0	m
1340	6 57 58.583	6 23 05.37	A,B	18.143	17.473	17.463	16.599	17.487	–	0.859	110.6 ± 0.2	n
1344	6 58 20.635	6 29 20.49	A,B	18.210	17.538	17.527	16.652	17.496	–	0.830	54.8 ± 0.5	n
1347	6 58 25.123	6 24 50.62	A,B	18.113	17.559	17.545	16.769	17.514	–	0.738	−8.4 ± 0.7	n
1349	6 58 06.074	6 20 55.42	A,B	–	–	–	–	17.521	–	0.834	105.2 ± 1.3	m
1350	6 58 07.071	6 29 51.00	A	–	–	–	–	17.534	–	0.735	−7.1 ± 0.8	n
1358	6 58 22.953	6 26 07.86	A,B	18.232	17.585	17.575	16.735	17.564	–	0.790	55.5 ± 1.4	n
1359	6 58 16.363	6 20 30.20	A,B	–	–	–	–	17.565	–	0.838	112.2 ± 0.7	n
1366	6 57 47.025	6 21 04.33	A,B	–	–	–	–	17.599	–	0.783	6.9 ± 2.5	n
1369	6 58 00.536	6 29 46.04	A,B	18.178	17.578	17.564	16.741	17.610	–	0.834	96.8 ± 2.3	n
1376	6 57 56.129	6 22 25.39	A,B	18.209	17.636	17.621	16.815	17.645	–	0.786	55.2 ± 0.8	n
1384	6 58 20.728	6 20 07.11	A,B	–	–	–	–	17.671	–	0.871	105.2 ± 0.7	m
1396	6 57 57.167	6 22 05.87	A,B	–	–	–	–	17.729	–	0.837	84.2 ± 0.7	n
1398	6 57 51.821	6 23 45.15	A,B	–	–	–	–	17.739	–	0.800	2.2 ± 3.0	n
1404	6 58 16.159	6 22 39.07	A,B	18.456	17.753	17.753	16.945	17.753	–	0.833	105.2 ± 1.3	m
1405	6 57 58.352	6 22 07.42	A,B	18.387	17.735	17.724	16.864	17.757	–	0.855	104.6 ± 0.84	m
1407	6 58 00.780	6 31 46.58	A,B	–	–	–	–	17.776	–	0.891	77.5 ± 0.3	n
1410	6 57 54.497	6 20 49.36	A,B	–	–	–	–	17.788	–	0.857	53.8 ± 3.7	n
1421	6 58 21.122	6 31 28.66	A,B	–	–	–	–	17.820	–	0.864	41.3 ± 2.4	n
1429	6 58 23.617	6 31 19.37	A,B	–	–	–	–	17.864	–	0.833	106.3 ± 1.3	m
1433	6 57 47.116	6 24 27.06	A,B	–	–	–	–	17.890	–	0.906	61.3 ± 0.9	n
1438	6 58 06.609	6 21 07.58	A	–	–	–	–	17.913	–	0.874	105.9 ± 1.3	m
1448	6 58 18.537	6 21 09.20	A,B	–	–	–	–	17.943	–	0.812	56.4 ± 1.4	n
1453	6 58 09.106	6 30 41.55	A,B	18.671	17.977	17.959	16.986	17.955	–	0.873	104.3 ± 0.6	m
1457	6 58 15.196	6 30 33.37	A,B	18.691	17.966	17.947	16.939	17.962	–	0.890	73.3 ± 0.5	n

velocity and membership flag (Cols. 11, 12). Giraffe was used in conjunction with the 316 lines/mm grating and order- sorting filter 15 (H15N) yielding a nominal resolving power $R = 17\,000$ and covering a spectral interval from 644.2 to 681.8 nm, including the Li I 670.8 nm line and several features to be used for radial velocity measurements.

Data reduction was performed using the Giraffe BLDRS pipeline[1], following the standard procedure and steps (Blecha et al. 2004). Sky subtraction was carried out separately; namely, we first computed the average sky ($sky_{av.}$) of three sets of five sky spectra and then derived the median of the three $sky_{av.}$. Radial velocities (RV) were derived from each single spectrum (see below). Spectra of stars that were not found to be RV variables were then co-added. Examples of final, sky-subtracted spectra are shown in Fig. 2. Final S/N range between 20 and 85, with an average value of ∼50.

3. Analysis

3.1. Radial velocities

Radial velocities were obtained from our spectra and used to derive membership information for the sample stars. The 645–682 nm region contains a large number of unblended lines (mainly Fe, Ca, Ti, and Ni) of various strengths suitable for accurate RV measurements. The individual lines used for the RV computation are listed in Table 2. The data analysis was performed by standard procedures within the IRAF package[2], fitting the strongest lines present in each spectrum by a Gaussian profile. The resulting RVs from the individual lines were averaged, and heliocentric corrections applied. Normally less than ten lines per spectrum allowed us to obtain an RV value with an error of about 2 km s^{-1}; RV values of spectra referring to the same star were then averaged for stars in configuration A having multiple exposures. Final radial velocities with their errors are given in Col. 9 of Table 1. For stars with multiple RV measurements, the error is the standard deviation from the average RV, while for stars in configuration B the error is the uncertainty in the RV measurement itself.

3.2. Li abundances

Lithium abundances were derived by measuring the equivalent width (EW) of the Li I line at 670.8 nm. Measurements were performed by direct integration below the continuum. For stars with detected Li, each measurement was performed twice, meaning we determined the maximum and minimum reasonable values. We then adopted the average between these two last values as EW measurement, and we used half of the difference between them as the error estimate on EW. In some RV members, the Li line could not be detected and we measured its upper limit, which was estimated as the EW of the smallest detectable feature in the Li spectral region. We measured the Li line in both radial velocity members and non-members. Whereas for most radial velocity members we detected the Li line, for six and 19 stars in fields A and B the S/N was too low to even infer a meaningful upper limit. We mention in passing that these stars are not

[1] version 1.12 – http://girbldrs.sourceforge.net/

[2] IRAF is distributed by the National Optical Astronomical Observatories, which are operated by the Association of Universities for Research in Astronomy, under contract with the National Science Foundation.

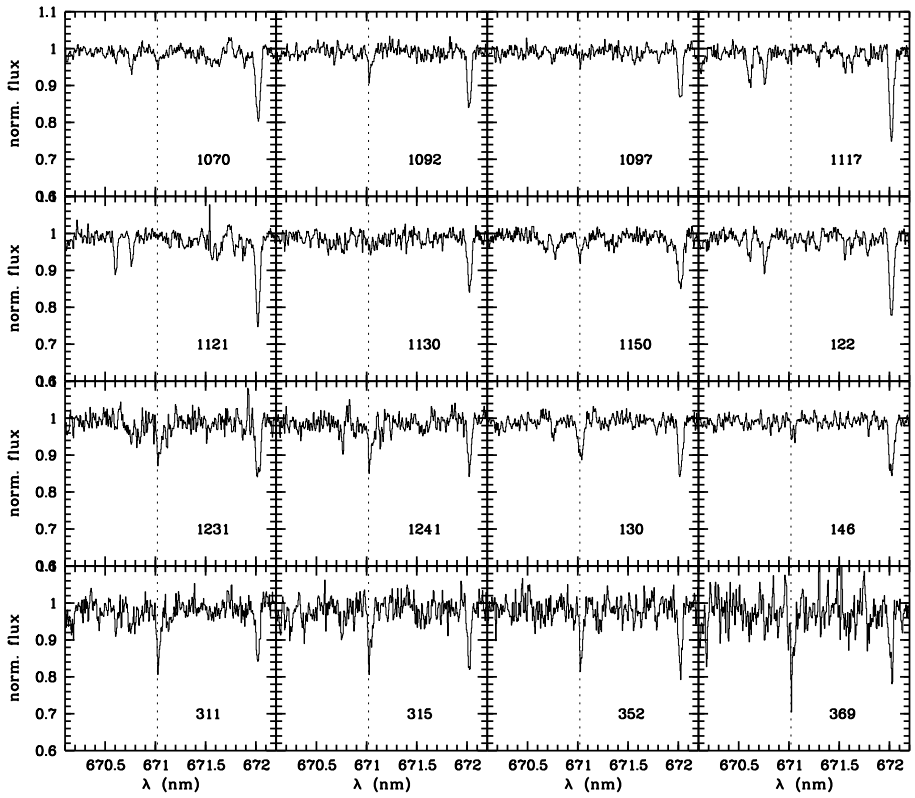

Fig. 2. Sample spectra in the Li region. The position of the Li line is marked.

Table 2. Individual lines suitable for RV computations.

Line & Multiplet	λ (Å)
CaI 19	6449.810
CaI 18	6462.566
CaI 18	6471.660
FeI 206	6475.632
FeI 168	6494.985
FeI 268 + Ti 102	6546.252
H_α	6562.808
FeI 268	6592.926
FeI 1197	6633.764
NiI 43	6643.641
FeI 111	6663.446
FeI 268	6677.993
LiI 1	6707.815
CaI 32	6717.687
FeI 111	6750.152
NiI 57	6767.778
FeI 205	6783.710
FeI 268	6806.851
FeI 1197	6810.280

necessarily fainter than those where the Li line was measurable. Lithium was also detected in 27 RV non-members.

Effective temperatures were determined on the basis of published photometry (Richtler & Sagar 2000; D'Orazi et al. 2006) and using the color versus temperature calibrations by Alonso et al. (1996 – for MS stars, 1999 – for evolved stars). When available, we used the photometry of D'Orazi et al., while we took colors from Richtler & Sagar for stars not included in the study of D' Orazi et al. As shown by Tosi et al. (2007), the agreement between the two photometries is very good for most stars in the magnitude range considered here. More specifically, we used $B-V$ colors from D' Orazi et al. (2006) for 45 stars out of the 47 for which they were available. Stars #364 and #1241 have $B-V$ colors from D'Orazi et al., but that of the former star is too red compared to the $V-I$, while $B-V$ of the latter is much bluer than the cluster sequence on the CM diagram; therefore we did not use $B-V$ from D'Orazi et al. We employed $B-V$ of Kaluzny & Mazur (1991) for two stars not included in the study of D'Orazi et al. (#236 and #333) and for the aforementioned star #364. Finally, for star #1241 and for eight stars without available $B-V$ we transformed $V-I$ into $B-V$ using a linear relationship that nicely fits the sequence of stars with both colors available. Reddening determinations towards Be 32 vary between $E(B-V) = 0.10$ and 0.18 mag (see Tosi et al. 2007); we assumed the value $E(B-V) = 0.14$, determined by Bragaglia et al. (2008) using spectroscopic temperatures, since we regard it as more reliable than values obtained from main sequence fitting.

To evaluate the random error that affects our temperature determinations, we compared effective temperatures based on the $B-V$ colors of D' Orazi et al. with those estimated from $B-V$ of Kaluzny & Mazur for the 32 stars studied in both referenced papers. The average $\Delta T_{\rm eff} = (T_{\rm eff}{}^{\rm D'Orazi} - T_{\rm eff}{}^{\rm K\&M})$ is −50 K with a standard deviation equal to 116 K. We adopt this value as the typical error on effective temperatures.

In previous studies (see Sestito & Randich 2005), we derived effective temperatures using the calibration of Soderblom et al. (1993a). Since this calibration does not have a term taking into account metallicity, we prefer to use Alonso's calibrations for Be 32, whose metallicity is below solar. Soderblom et al.'s calibration would have given warmer temperatures, with a typical difference of 144 K. However, at solar metallicity the two scales are very similar.

As is well known, at our resolution the Li line is blended with a Fe I line. To estimate the contribution of Fe to the total EW, we cannot use the analytical approximation of Soderblom et al. (1993b), which was derived using stars with solar metallicity. We instead estimated the EW of this feature employing MOOG

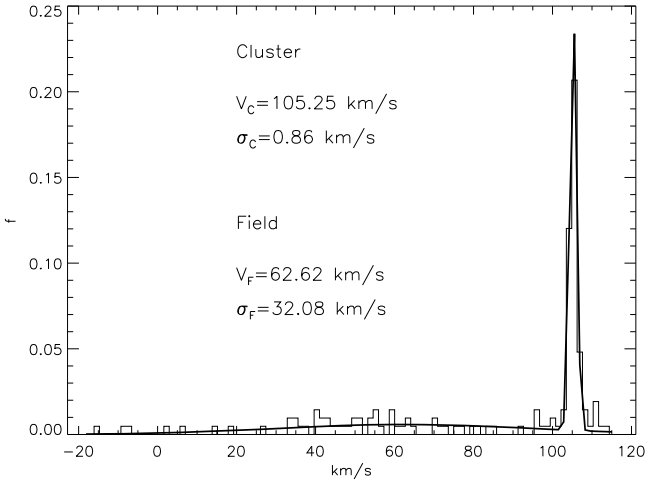

Fig. 3. Density distribution of radial velocities for the 153 stars for which we could get a measurement. The two Gaussians (solid curves) indicate the best fits for the cluster and field, respectively. The average velocities along with 1σ dispersion are indicated.

(Sneden 1973 – Version 2000) and the driver *ewfind* using the appropriate metallicity and stellar parameters. Effective temperatures were derived as described above. The surface gravity for evolved stars was estimated in the same fashion as in Sestito et al. (2006), while for stars on the MS we assumed $\log g = 4.5$. Microturbulence values $\xi = 1.1$ and 1.5 km s^{-1} were used for unevolved and evolved stars, respectively. We found that for MS objects EW(Fe 6707.44) = (22.5–3.3 $\times$ $10^{-3}\times T_{\rm eff}$) Å, while the EW of the Fe line was computed separately for each evolved star. The strength of this very weak Fe line has a very weak dependence on both the microturbulence ξ and $\log g$: a change in ξ of 1 km s^{-1} results in a change in EW below 0.2 mÅ, while a change of 0.5 dex in log g results in a difference of ~0.2 mÅ.

The Li abundances were derived from corrected EWs using Soderblom et al. (1993b) curves of growth (COGs), which assume local thermodynamic equilibrium (LTE). A correction for non-LTE effects following Carlsson et al. (1994) has also been run on our data, but it produces no significant changes. Li for evolved stars was instead derived using MOOG, which allows changing surface gravity and microturbulence. Using of a different code and method to derive Li for evolved and unevolved stars introduces a small offset between the two abundance scales. By using MOOG, we would obtain slightly higher log n(Li) for dwarf stars, typically by 0.05–0.1 dex. On the one hand, this offset does not affect our results and, in particular, our conclusions on dilution in more evolved stars (Figs. 5 and 6); on the other hand, the use for Be 32 dwarf members of the same COGs employed in the literature for other OCs is critical to correctly draw the time evolution of Li.

The final error on the Li abundance measurement is computed by summing quadratically the contributions from EW and temperature. Errors in the Fe I contribution due to errors in $T_{\rm eff}$ are very small, much smaller than the errors in the EW measurements themselves: namely, δEW(Fe I) = 0.5 mÅ for $\delta T_{\rm eff}$ = 100 K.

4. Results

4.1. Radial velocities and membership

In Fig. 3, we show the density distribution of radial velocities for the 153 stars for which we were able to measure them. The figure clearly shows a very narrow peak that indicates the presence of the cluster. To derive the average cluster radial velocity, we fitted the observed distribution with two Gaussians, one for the cluster and one for the field, and determined the best fit using a maximum likelihood algorithm. We obtained $\rm RV_{cluster}$ = 105.2 km s^{-1}, $\sigma_{\rm cluster}$ = 0.86 km s^{-1} and $\rm RV_{field}$ = 62.6 km s^{-1}, $\sigma_{\rm field}$ = 32.1 km s^{-1}, respectively. Our measurement of the RV is in good agreement with the values of D' Orazi et al. (2006, RV = 106.7 ± 8.5 km s^{-1}) from low-resolution spectroscopy of 48 stars brighter than the turn-off, of Sestito et al. (2006, RV = 106 ± 1.4 km s^{-1}), and of Scott et al. (1995, 106 ± 10 km s^{-1}) from the intermediate-resolution spectroscopy of 10 giants. Also, three stars in our sample have an RV measurement from D'Orazi et al.: #74 (their #698), #97 (their #113), and #1090 (their #364). The agreement in RV is excellent for all of them. We stress that, thanks to our large sample, we have been able to constrain the internal dispersion in velocity much better than in previous studies, pushing it to below 1 km s^{-1}.

We considered all stars as cluster members with RV within 3σ from the cluster average: adopting this criterion, 59 and 24 stars turned out to be members in fields A and B. The total fraction of members is 83/153 stars, i.e., 54%. The expected number of contaminants, or non members with RV consistent with the cluster, is 2 stars. Since our observations were obtained within the same night, we have only been able to identify one possible binary systems (star #1090). This system has average velocity consistent with membership, but a double-line system and larger-than-average deviation around the mean. We have tentatively classified it as an SB2 cluster member. Most likely, additional unidentified binaries might be present among stars with RV discrepant with membership and detected Li line. Further follow-up is needed to confirm their membership. Therefore, we regard the fraction of members as a lower limit to the real value. The "cleaned" CM diagrams are shown in Fig. 4, where RV members and non-members and the SB2 binary are denoted with different symbols. Whereas we refer to Tosi et al. (2007) for a detailed discussion of the analysis of the cluster CM diagram, we mention here that our membership determination has allowed us to clean the turn-off region, thus allowing a more solid derivation of cluster parameters, as done by Tosi et al. Among the subgiants we note the presence of two confirmed members (one in the V vs. $B-V$ diagram) somewhat fainter than the cluster sequence. We do not have any explanation for them, but suggest that they might be the two expected contaminants.

4.2. Lithium abundances

In Table 3 we list confirmed members (from Table 1) for which we were able to either measure the EW of the Li line or infer a reasonable upper limit. In the table we provide IDs (same as in Table 1), dereddened $B-V$ colors, effective temperatures, measured Li equivalent widths, and Li abundances. The last are in the usual notation $\log n(\rm Li) = \log N(\rm Li)/N(\rm H)+12$. In Fig. 5a we plot the V–$V-I$ diagram of cluster members with different symbol sizes denoting stars with different Li contents, while in Fig. 5b we show Li abundances as a function of V magnitude. The figures very well illustrate the evolution of Li along the CM diagram. All stars on the MS and at the TO have Li abundances larger than log n(Li) = 2 and their present Li abundance is the result of MS depletion; on the other hand, cluster members slightly more evolved than TO have started diluting their surface Li, due to the deepening of the convective zone (e.g., Randich et al. 1999). The transition between stars that have and that have not undergone dilution occurs in a very narrow magnitude range

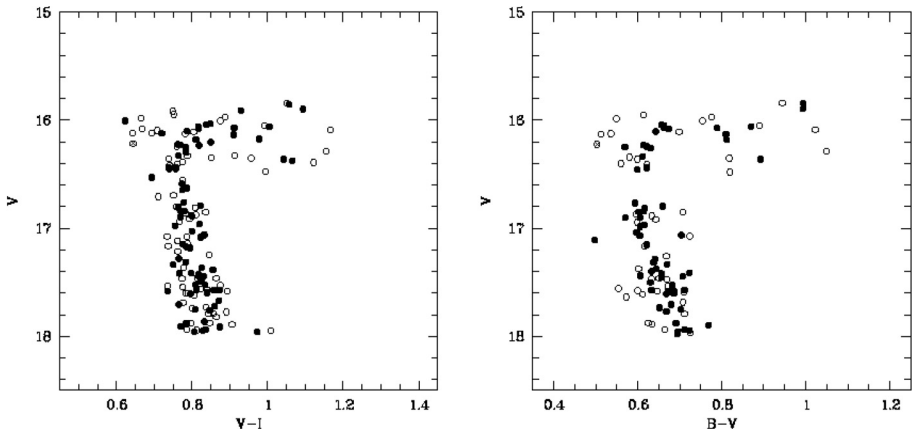

Fig. 4. "Cleaned" color–magnitude diagrams. Open symbols represent all observed stars, while filled symbols denote radial velocity members. The crossed symbol denotes the possible SB2 binary. When available we have considered photometry from D'Orazi et al. (2006), while in the other cases we have considered $B - V$ colors from Kaluzny & Mazur (1991) and $V - I$ colors from Richtler & Sagar (2000).

(see also Pasquini et al. 2004). Dilution progressively continues along the subgiant branch, up to a Li abundance ∼1. In Fig. 6 we show the usual plot of Li abundances as a function of effective temperature for unevolved cluster stars (TO and MS) and compare Be 32 with the much younger and more metal-rich Hyades (upper panel) and with both the slightly younger M 67 and the slightly older cluster NGC 188 (lower panel). Both NGC 188 and M 67 OCs have a solar metallicity (Randich et al. 2003, 2006), and thus are a factor of ∼2 more metal rich than Be 32. Lithium abundances for the three OCs were taken from the compilation of Sestito & Randich (2005). In that paper Li abundances had been derived using the same COGs and NLTE correction employed here.

The figure shows that, at variance with the Hyades and M 67, but more like NGC 188, Be 32 distribution does not show any major trend of decreasing Li abundance with decreasing $T_{\rm eff}$. We find average Li abundance values of log n(Li)= 2.63 ± 0.17, 2.62 ± 0.07, and 2.47 ± 0.16 for stars in the temperature ranges $T_{\rm eff} > 6200$ K, $6200 \geq T_{\rm eff} \geq 6000$ K, and $T_{\rm eff} < 6000$ K. The three average values are, within the errors, the same. Also, at variance with M 67, but similar to NGC 188, the Be 32 sample is not characterized by any significant (larger than errors) dispersion in Li. More specifically, Figs. 5b and 6 show that the maximum star-to-star difference for unevolved stars is on the order of 0.5 dex. Assuming Gaussian statistics, this corresponds to a 1σ dispersion of ∼0.15 dex, comparable to the average error in log n(Li). Given the large size of our sample, we regard the lack of a significant scatter as real and not due to low number statistics and conclude that the appearance of the spread among open cluster stars is an exception rather than the rule, since the majority of OCs do not show it. Most important, whereas Hyades stars warmer than ∼6000 K are somewhat more Li-rich than their Be 32 counterparts, the Li distributions of cooler stars are almost indistinguishable. The log n(Li)–$T_{\rm eff}$ of NGC 188 and Be 32 patterns are also very similar and close to the upper envelope of M 67. In other words, the comparison of OCs of different ages and metallicity shows that, with the exceptions of the severely Li-depleted stars in the lower envelope of M 67, stars in the ∼6000–5700 K $T_{\rm eff}$ range seem to converge to a very similar value of Li abundance.

5. Discussion

5.1. Pop. I plateau

The present study allows us to make firm conclusions about the empirical evolution of Li abundance during the MS of stars with temperatures (but not necessarily masses – see next section) similar to the Sun. In Fig. 7 we show the mean Li abundance as a function of age for stars in the 6050–5750 temperature range. The figure was done using the data of Sestito & Randich (2005), to which we added the average Li abundance of the ∼1 Gyr old NGC 3960 (from Prisinzano & Randich 2007) and the average for Be 32 inferred here. As already discussed by Sestito & Randich, stars in this $T_{\rm eff}$ interval undergo a smooth, but continuous Li depletion during the first ∼600 Myr on the main sequence, on a typical timescale of ∼1.4 Gyr. As already mentioned, at older ages depletion becomes bimodal: it continues for a fraction of stars, while it stops for the majority of stars and the average log n(Li) converge to a plateau, which is quantitatively – and surprisingly – close to the plateau of Pop. II stars. The evidence for this Pop. I plateau is statistically confirmed by the inclusion in the sample of the Be 32, for which we derived an average abundance log n(Li) = 2.47 ± 0.16. This value is, slightly higher, but within the margins of error consistent, with that of the intermediate age OCs (2.33 ± 0.17), the upper envelope of M 67 (2.25 ± 0.12), and NGC 188 (2.34 ± 0.14). As to the Pop. II plateau, values range between a minimum of 2.10 ± 0.09 (Bonifacio et al. 2007) and a maximum of ∼2.4 (Meléndez & Ramirez 2004). The conclusion is that Pop. I stars are not necessarily heavily Li-depleted, even at very old ages. The major consequence is that Li cannot be used as an age indicator for stars older than ∼500 Myr: a lithium abundance in the interval log n(Li) ∼2.3–2.6 does not allow discerning whether a star is 0.5 or 6 Gyr old. The above points are to be kept in mind when deriving the properties, age in particular, of stars hosting extrasolar planets. On the other hand, the Sun represents an exception and is not representative of Li depletion in solar-type stars, since it has undergone a larger-than-normal depletion. We believe that low Li (a factor greater than 30–50 depletion) should be regarded as indicative of a peculiar, but similar-to-the Sun, evolution.

5.2. Lithium as a function of stellar mass

Figure 6 clearly shows that the amount of Li depletion at a given $T_{\rm eff}$ does not depend on the cluster metallicity. The lack of any Li-metallicity dependence has already been discussed by Sestito & Randich (2005) on empirical grounds and by Piau et al. (2003) on theoretical grounds. The latter study show that metallicity variations on the order of 0.1 dex result in changes of both $T_{\rm eff}$ and temperature at the basis of the convective zone ($T_{\rm BCZ}$); however, the relationship between $T_{\rm eff}$ and $T_{\rm BCZ}$, and thus the amount of depletion at a given $T_{\rm eff}$, remain almost unaltered. The inclusion of Be 32 in the open cluster sample and the

Table 3. Final results of our analysis.

ID	$(B-V)_0$	$T_{\rm eff}$ (K)	EW(Li) (mÅ)	log n(Li)
97	0.730	5233	40 ± 10	1.53 ± 0.15
109	0.522	6024	≤16	≤1.88
117	0.670	5401	42 ± 6	1.76 ± 0.14
122	0.672	5395	≤25	≤1.59
130	0.490	6152	66 ± 7	2.73 ± 0.12
146	0.481	6189	55 ± 5	2.66 ± 0.11
154	0.459	6282	58 ± 12	2.77 ± 0.15
193	0.454	6303	38 ± 7	2.57 ± 0.15
206	0.477	6206	60 ± 7	2.72 ± 0.11
216	0.430	6408	63 ± 2	2.92 ± 0.13
231	0.466	6252	47 ± 2	2.63 ± 0.13
236	0.560[a]	5878	48 ± 3	2.31 ± 0.15
241	0.481	6189	57 ± 4	2.68 ± 0.14
265	0.530	5992	76 ± 6	2.67 ± 0.10
271	0.498	6119	59 ± 7	2.64 ± 0.12
276	0.504	6095	51 ± 9	2.54 ± 0.13
277	0.466	6252	47 ± 6	2.63 ± 0.10
278	0.516	6047	57 ± 6	2.56 ± 0.12
288	0.583	5793	53 ± 4	2.28 ± 0.10
289	0.567	5852	43 ± 6	2.23 ± 0.12
299	0.542	5946	65 ± 6	2.54 ± 0.11
311	0.546	5931	58 ± 6	2.46 ± 0.12
313	0.500	6111	60 ± 9	2.64 ± 0.13
314	0.493	6140	59 ± 1	2.66 ± 0.16
315	0.546	5931	74 ± 7	2.60 ± 0.11
316	0.528	6000	83 ± 13	2.73 ± 0.14
325	0.533	5981	63 ± 8	2.55 ± 0.13
333	0.540 [a]	5954	60 ± 10	2.50 ± 0.14
352	0.528	6000	70 ± 11	2.63 ± 0.14
357	0.551	5912	46 ± 7	2.32 ± 0.17
364	0.580[a,*]	5804	49 ± 7	2.25 ± 0.14
369	0.555	5897	93 ± 4	2.71 ± 0.15
371	0.571	5837	84 ± 12	2.59 ± 0.14
374	0.583	5793	50 ± 10	2.25 ± 0.15
1050	0.853	4920	65 ± 5	1.45 ± 0.16
1070	0.522	6024	25 ± 7	2.12 ± 0.25
1092	0.473	6222	33 ± 5	2.44 ± 0.15
1113	0.472	6227	38 ± 3	2.51 ± 0.15
1121	0.753	5233	≤17	≤1.82
1128	0.450[b]	6320	31 ± 6	2.49 ± 0.14
1130	0.450[b]	6320	≤20	≤2.27
1150	0.480[b]	6193	55 ± 5	2.56 ± 0.12
1212	0.475	6214	55 ± 7	2.68 ± 0.12
1228	0.465	6256	63 ± 4	2.79 ± 0.12
1231	0.457	6290	56 ± 6	2.76 ± 0.11
1241	0.530[b,*]	5992	52 ± 5	2.46 ± 0.11
1257	0.490[b]	6152	53 ± 9	2.61 ± 0.12
1263	0.490[b]	6152	60 ± 7	2.68 ± 0.12
1279	0.501	6107	61 ± 10	2.65 ± 0.13
1300	0.493	6140	42 ± 6	2.48 ± 0.12
1327	0.516	6047	37 ± 10	2.34 ± 0.19
1337	0.490	6152	44 ± 5	2.51 ± 0.12
1349	0.530[b]	5992	85 ± 9	2.74 ± 0.12
1384	0.570[b]	5841	59 ± 6	2.39 ± 0.12
1405	0.512	6063	65 ± 10	2.64 ± 0.14
1438	0.570[b]	5841	70 ± 12	2.48 ± 0.15
1453	0.554	5900	49 ± 9	2.34 ± 0.15

[a]: $B-V$ from Richtler & Sagar (2000); [b]: $(B-V)_0$ derived from $(V-I)$ (see text); [*]: $B-V$ from D'Orazi et al. available, but not used (see text).

comparison with the Hyades shows that this holds true for metallicity differences as large as 0.4–0.5 dex.

As is well known, however, metallicity does affect stellar structure: specifically, for a given mass, lower metallicities correspond to higher $T_{\rm eff}$. In contrast, for a given effective temperature, lower metallicity stars have lower masses and stars with the same, close-to solar temperature, do not have the same, solar mass, if their metal content is different. In order to investigate Li depletion as a function of mass, we derived masses for unevolved stars in Be 32, as well as for the Hyades, M 67, and NGC 188 using the Padova isochrones (Girardi et al. 2000 – http://pleiadi.pd.astro.it/) and the appropriate metallicities. When needed, we interpolated between different isochrones. In Fig. 8 we compare Li abundances as a function of mass for unevolved stars in Be 32 with the Hyades, M 67, and NGC 188 members. The range covered by Pop. II stars is also shown. This figure indicates that the distributions of the different OCs no longer overlap in the log n(Li) – mass diagram as it was instead the case for the log n(Li)–$T_{\rm eff}$ plane. This is due to the fact that Be 32 stars with temperatures close to solar are less massive than the Sun, of their counterparts in the solar metallicity NGC 188 and M 67, and of their metal-rich counterparts in the Hyades. The figure proves that Be 32 members at all masses have depleted less Li than stars with similar mass in the other old OCs; also, focusing on star with mass close to solar, the figure shows that NGC 188 members and the upper envelope of M 67 have depleted the same Li as their more metal-rich Hyades counterparts. In summary, both the timescales and the amount of Li depletion are different for stars with the same mass and different metallicities. This result indicates that, when looking at masses, metallicity affects the amount of depletion at a given age. In contrast, we stress again that the evolution of star with the same $T_{\rm eff}$ does not depend on [Fe/H] (at least within ±0.2–0.3 dex from the solar value), since more metal-poor and less massive stars, have the same internal structure of solar-metallicity, solar-mass ones.

5.3. Comparison with model predictions

For a formally correct comparison of the empirical evolution of Li with model predictions at a given mass, one should not mix data of OCs with significantly different metallicities or, alternatively, the appropriate metallicity should be considered. However, we believe that the comparison between model predictions and empirical evolution in a given temperature range can still be performed, since, at least as far as Li is concerned, the evolution of stars with similar temperatures, but different masses and metallicities is virtually the same. As an example, we show again in Fig. 9 the mean Li abundance as a function of age (see Fig. 7) and compare it with the predictions of the models by Charbonnel & Talon (2005), which include both rotational mixing and gravity waves. The figure indicates that these models reproduce the observed distribution up to 1 Gyr rather well. Also, the models with initial rotational velocity 50–80 km s^{-1} are in good agreement with the datapoints corresponding to the lower envelopes of M 67 and with the solar datapoint. However, even the model with the lowest initial rotation is not able to fit the plateau in Li. In conclusion, while all classes of models including extra-mixing processes predict that, once they start causing Li depletion, they continue being efficient throughout the permanence on the MS, observational evidence indicates that this is not the case at all. To our knowledge, none of the models proposed so far predicts the convergence of Li at old ages. We note that, when comparing model predictions with observations, we assumed that all OCs have the same initial (meteoritic) Li abundance. The assumption that the initial Li is instead higher in

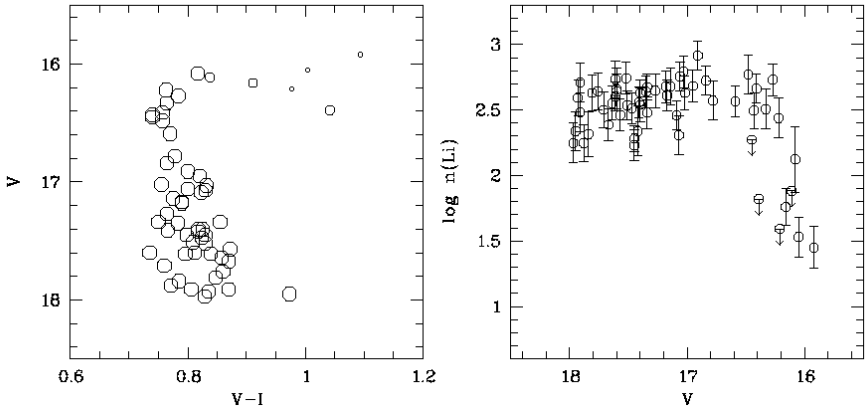

Fig. 5. *Panel* **a)** $V - V - I$ diagram of confirmed cluster members. Different symbol sizes indicate different Li abundance bins; namely, from the largest to the smallest ones: log n(Li) ≥ 2.0, 2.0 ≤ log n(Li) < 1.7, and log n(Li) < 1.7. For 47 of the 57 stars with a Li measurement, we have considered photometry from D'Orazi et al. (2006), while for the remaining 10 stars not included in the D'Orazi et al. study, we used Richtler & Sagar (2000) magnitudes and colors. *Panel* **b)**: Lithium abundance – log n(Li), in the usual logarithmic scale where n(H) = 12 – as a function of V magnitude for confirmed cluster members.

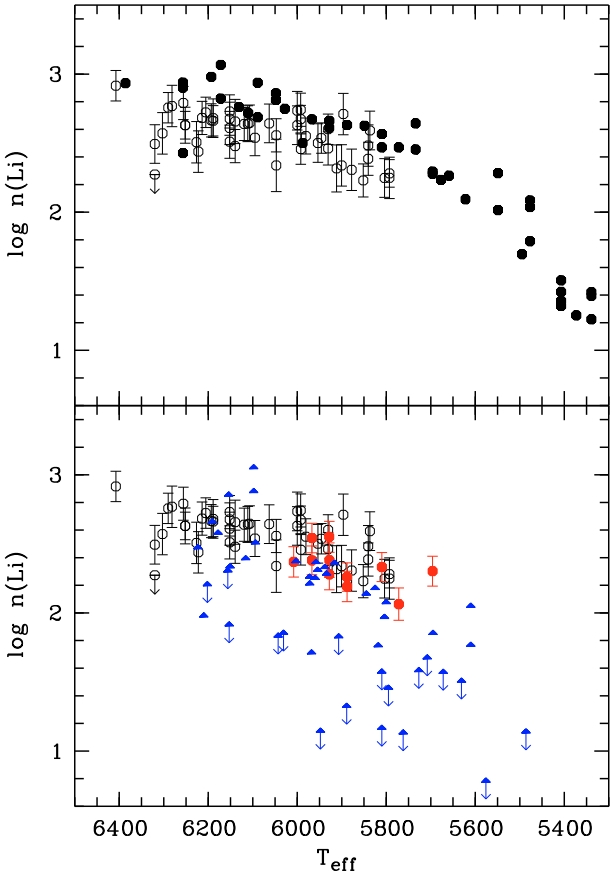

Fig. 6. *Upper panel*: comparison of the distribution of log n(Li) as a function of $T_{\rm eff}$ for unevolved stars in Be 32 (open circles) and the Hyades (filled circles); *lower panel*: same as *upper panel*, but Be 32 is compared to M 67 (filled triangles) and NGC 188 (filled circles).

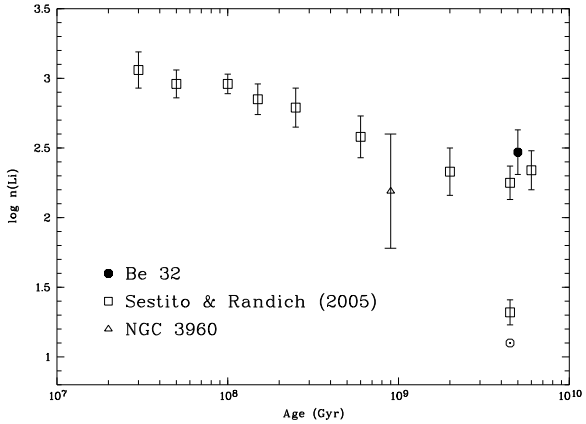

Fig. 7. Average Li abundance as a function of age for stars in the 5750–6050 K interval. Open squares are OCs from Sestito and Randich (2005), the open triangle represents the average for NGC 3960 Prisinzano & Randich (2007), while the filled circle denotes Be 32. For M 67 the average of the upper and lower envelopes are plotted. The Sun is also shown in the figure.

young OCs would imply a different normalization of theory vs. models and a better fit of the very old OCs; still, the disagreement between the observed convergence and the models, which keep decreasing at old ages, remains.

5.4. Pop. I and Pop. II plateaus

In the previous sections we have definitively shown that stars with temperatures similar to the Sun are not necessarily heavily Li-depleted like the Sun is; instead, Li abundances of the majority of stars converge towards a plateau, whose value, on the order of log n(Li) = 2.3–2.5, is close (although not identical) to that of Pop. II stars. However, the path/masses/timescales are different towards virtually this same average value of Li. The similarity of the plateau of Pop. I stars to the plateau of the significantly more metal-poor Pop. II is indeed very intriguing and should be investigated on theoretical grounds. Figure 8 indeed suggests that there might be a sequence between old, solar-metallicity OCs and metal–poor less massive Pop. II stars, with Be 32 in the middle. This sequence is purely phenomenological and it does not provide insight into the depletion history of Pop. II stars or into whether they actually depleted some Li or not; nevertheless, it is tempting to interpret it as evidence that, whatever the initial Li abundance and whatever the mixing mechanism, the final Li abundance is the same for metal-poor Pop II stars and more metal-rich ones. Those stars, like the Sun, that instead deplete a much larger amount of Li represent an exception.

6. Conclusions

We carried out a FLAMES/Giraffe survey of almost 160 candidate members of the old, metal-poor open cluster Be 32, with the goals of inferring membership and of studying the Li abundance pattern. To this aim, we derived radial velocities and Li abundances. Slightly more than half of the sample stars are confirmed as cluster members. This is a lower limit, since we may have

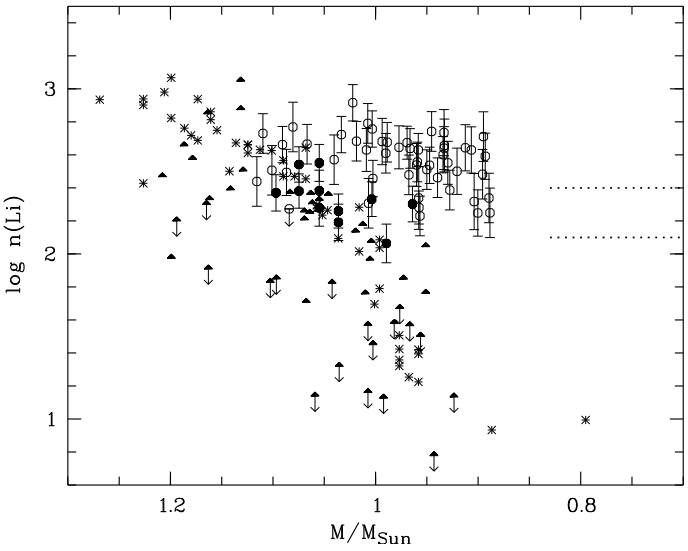

Fig. 8. log n(Li) as a function of mass for Be 32 (open circles), the Hyades (asterisks), M 67 (filled triangles), and NGC 188 (filled circles). The horizontal lines delimits the range covered by Pop. II stars considering the lowest and highest values of the plateau.

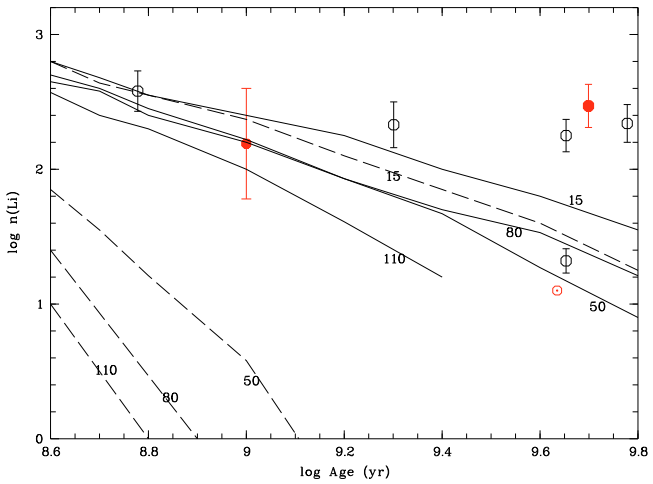

Fig. 9. Same as Fig. 7, but a narrower age interval is shown. The empirical distribution is compared with the predictions of the models by Charbonnel & Talon (2005). The latter have been reconstructed starting from Fig. 2 in that paper. Different curves are for different initial rotational velocities (in km s^{-1}) as labeled. Solid curves correspond to model including waves + rotation, while dashed lines denote models including only waves.

missed some binaries due to the too short time coverage of our observations. The Li versus $T_{\rm eff}$ distribution of unevolved members overlaps with that of the slightly older, more metal-rich NGC 188, and with the upper envelope of M 67. At variance with the last, Be 32 does not show any dispersion in Li. The average abundance of stars with solar–like *temperature* is slightly below the Hyades but, within the margins of error, the same as for their counterparts in the intermediate age OCs, the upper envelope of M 67, and NGC 188. This confirms, on solid and statistically significant grounds, that, with exception of Li-poor stars like the Sun, Li abundances in solar-like Pop. I stars converge towards a plateau value, implying that Li cannot be used as an age indicator after about 0.5 Gyr. In addition, the plateau of old OCs is close to the plateau value of Pop. II stars. To our knowledge, none of the models including extra-mixing developed so far predicts the convergence toward a plateau at old ages.

Given their lower metallicity, Be 32 stars with temperature close to the Sun are less massive than the Sun. A comparison in a log n(Li)–mass diagram shows that these stars have depleted much less Li than the Hyades with similar mass. Our conclusion is that stars with different masses and metallicities, but very similar temperatures, converge at old ages to the same Li abundance, though following different Li depletion histories. This might also be true for halo stars.

Acknowledgements. We are grateful to Paolo Spanò for help with the maximum-likelihood analysis of radial velocities and to Paolo Montegriffo for providing the software to cross-correlate catalogs. We thank the referee, Andreas Korn, for very useful suggestions. This work has made extensive use of the services of WEBDA, ADS, CDS, etc. S. Randich has been supported by an INAF grant on *Young clusters as probes of star formation and early stellar evolution.*

References

Alonso, A., Arribas, S., & Martinez-Roger, C. 1996, A&A, 313, 873
Alonso, A., Arribas, S., & Martinez-Roger, C. 1999, A&AS, 140, 261
Blecha, A., & Simond, G. 2004, Technical report, GIRAFFE BLDR Software – Reference Manual Version 1.12, Observatoire de Genève
Bonifacio, P., Molaro, P., Sivarani, T., et al. 2007, A&A, 462, 851
Bragaglia, A., Sestito, P., Villanova, S., et al. 2008, A&A, 480, 79
Brun, A. S., Turck-Chièze, S., & Zahn, J.-P. 1999, ApJ, 525, 1032
Carlsson, M., Rutten, R. J., Bruls, J. H. M. J., & Shchukina, N. G. 1994, A&A, 288, 860
Chaboyer, B., Demarque, P., & Pinsonneault, M. H. 1995, ApJ, 441, 865
Charbonnel, C., & Talon, S. 1999, A&A, 351, 635
Charbonnel, C., & Talon, S. 2005, Science, 309, 2189
Cyburt, R. H., Fields, B. D., & Olive, K. A. 2003, Phys. Lett. B, 567, 227
Dean, J. F., Warren, P. R., & Cousins, A. W. J. 1978, MNRAS, 183, 569
Deliyannis, C. P., & Pinsonneault, M. 1997, ApJ, 488, 833
D' Orazi, V., Bragaglia, A., Tosi, M., Di Fabrizio, L., & Held, E. V. 2006, MNRAS, 368, 471
Eddington, A. S. 1925, The Observatory, 48, 73
Garcia López, R. J., & Spruit, H. C. 1991, ApJ, 377, 268
Hasegawa, T., Malasan, H. L., Kawakita, H., et al. 2004, PASJ, 56, 295
Girardi, L., Bressan, G., Bertelli, G., & Chiosi, C. 2000, A&AS, 141, 371
Kaluzny, J., Mazur, B., 1991, AcA, 41, 167
Korn, A., Grundahl, F., Richard, O., et al. 2006, Nature, 442, 657
Korn, A., Grundahl, F., Richard, O., et al. 2007, ApJ, 671, 402
Meléndez, J., & Ramirez, I. 2004, ApJ, 615, L33
Michaud, G. 1986, ApJ, 302, 650
Michaud, G., Richard, O., Richer, J., & Vandenberg, D. 2004, ApJ, 606, 452
Montalbán, J., & Schatzmann, E. 2000, A&A, 354, 943
Pasquini, L., Randich, S., & Pallavicini, R. 1997, A&A, 325, 535
Pasquini, L., Randich, S., Zoccali, M., et al. 2004, A&A
Piau, L., Randich, S., & Palla, F. 2003, A&A, 408, 1037
Prisinzano, L., & Randich, S. 2007, A&A, 475, 539
Randich, S., Gratton, R., Pallavicini, R., Pasquini, L., & Carretta, E., 1999, A&A, 348, 487
Randich, S., Sestito, P., & Pallavicini, R. 2003, A&A, 399, 133
Randich, S., Sestito, P., Primas, F., Pallavicini, R., & Pasquini, L., 2006, A&A, 450, 557
Richtler, T., & Sagar, R. 2001, Bull. Astr. Soc. India, 29, 53
Scott, J. E., Friel, E. D., & Janes, K. A. 1995, AJ, 109, 1706
Sestito, P., & Randich, S. 2005, A&A, 442, 615
Sestito, P., Bragaglia, A., Randich, S., et al. 2006, A&A, 458, 121
Sneden, C. 1973, ApJ, 184, 839
Soderblom, D. R., Stauffer, J. R., Hudon, J. D., & Jones, B. F. 1993a, ApJS, 85, 313
Soderblom, D. R., Jones, B. F., Balachandran, S., Stauffer, J. R., et al. 1993b, AJ, 106, 1059
Spergel, E. A., & Zahn, J.-P. 1992, A&A, 265, 106
Spergel, D. N., Bean, R., Doré, O., et al. 2007, ApJS, 170, 377
Spite, M., & Spite, F. 1982, A&A, 115, 357
Steigman, G. 2006, in Chemical Abundances and Mixing in Stars in the Milky Way and its Satellites, ed. S. Randich, & L. Pasquini (Springer), 331
Tosi, M., Bragaglia, A., & Cignoni, M. 2007, MNRAS, 378, 730
Talon, S. 2008, Mem. SAIt , 79, 569
Zahn, J.-P. 1974, IAUS, 59, 185
Zahn, J.-P. 1992, A&A, 265, 115